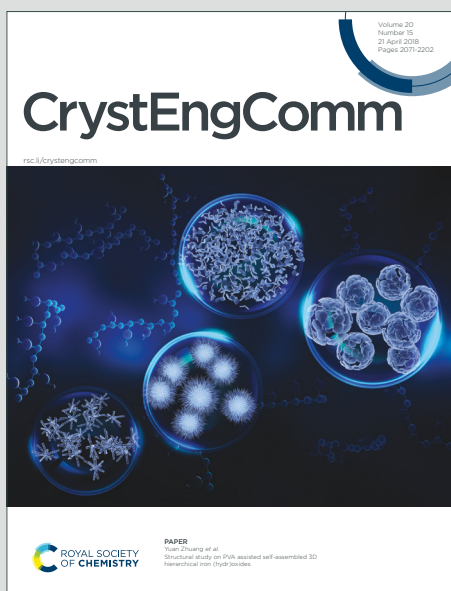


# CrystEngComm

Accepted Manuscript

This article can be cited before page numbers have been issued, to do this please use: M. N. Ahmed, M. Madni, S. Anjum, S. Andleeb, S. Hameed, A. M. Khan, M. Ashfaq, M. N. Tahir, A. Frontera and D. M. Gil, *CrystEngComm*, 2021, DOI: 10.1039/D1CE00256B.



This is an Accepted Manuscript, which has been through the Royal Society of Chemistry peer review process and has been accepted for publication.

Accepted Manuscripts are published online shortly after acceptance, before technical editing, formatting and proof reading. Using this free service, authors can make their results available to the community, in citable form, before we publish the edited article. We will replace this Accepted Manuscript with the edited and formatted Advance Article as soon as it is available.

You can find more information about Accepted Manuscripts in the [Information for Authors](#).

Please note that technical editing may introduce minor changes to the text and/or graphics, which may alter content. The journal's standard [Terms & Conditions](#) and the [Ethical guidelines](#) still apply. In no event shall the Royal Society of Chemistry be held responsible for any errors or omissions in this Accepted Manuscript or any consequences arising from the use of any information it contains.

## ARTICLE

## Crystal engineering with pyrazolyl-thiazole derivatives: Structure-directing role of $\pi$ -stacking and $\sigma$ -hole interactions

Received 00th January 20xx,  
Accepted 00th January 20xx

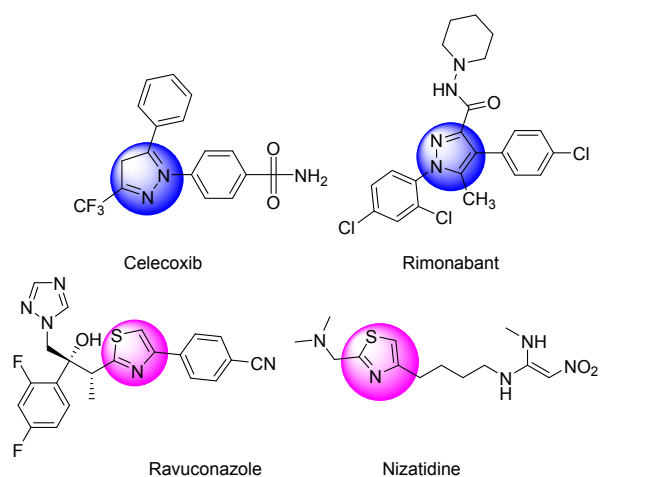
DOI: 10.1039/x0xx00000x

Muhammad Naeem Ahmed<sup>a,\*</sup>, Murtaza Madni<sup>b,\*</sup>, Shaista Anjum<sup>a</sup>, Saiqa Andleeb<sup>c</sup>, Shahid Hameed<sup>b</sup>, Abdul Majeed Khan<sup>d</sup>, Muhammad Ashfaq<sup>e</sup>, Muhammad Nawaz Tahir<sup>e</sup>, Diego M. Gil<sup>f</sup> and Antonio Frontera<sup>g,\*</sup>

The synthesis and X-ray characterization of 1-(2-(3-(4-bromophenyl)-5-(4-methoxyphenyl)-4,5-dihydro-1H-pyrazol-1-yl)-4-methylthiazol-5-yl)ethanone (**7**), ethyl 2-(5-(4-bromophenyl)-3-(4-chlorophenyl)-4,5-dihydropyrazol-1-yl)thiazole-4-carboxylate (**8**) and 2-(5-(4-chlorophenyl)-3-phenyl-4,5-dihydro-1H-pyrazol-1-yl)-N'-(2-hydroxy-3-methoxybenzylidene)thiazole-4-carbohydrazide (**10**) is described in this manuscript. The structure-directing role of a variety of noncovalent interactions have been analyzed energetically using DFT calculations and by means of Hirshfeld-surface analysis. Moreover, the existence and importance of halogen and chalcogen bonding interactions have been analyzed by using the quantum theory of "atoms-in-molecules" and the noncovalent interaction index (NCIplot).

### Introduction

Compounds with pyrazole moieties play an important role in active pharmaceutical drugs and agrochemicals in controlling infections, diseases and pests.<sup>1-3</sup> There are several drugs in recent years that have been developed from pyrazole derivatives. For example, celecoxib demonstrates anti-inflammatory effects and inhibits COX-2; rimonabant functions as a cannabinoid receptor and is also used to treat obesity.<sup>4</sup> Moreover pyrazole derivatives have shown significant biological activities such as antimicrobial, analgesic, anti-inflammatory, and anticancer activities.<sup>5-7</sup> The significance of thiazoles is emphasized by the fact that they are precursors for the synthesis of several drugs, such as ravuconazole<sup>8</sup> an antifungal agent, and nizatidine<sup>9</sup> as an antiulcer agent (Scheme 1). Besides, thiazole group is also important in drug designing, since it frequently appears in the structures of various natural products and biologically active compounds like thiamine and also in some antibiotic drugs like penicillin, micrococin and many metabolic products of fungi and primitive marine animals.



Scheme 1. Structure of Celecoxib, romonabant, ravuconazole and nizatidine

In addition, combined pyrazolyl-thiazole scaffolds are also relevant for several medical and pharmaceutical applications. Their derivatives are potent antiviral<sup>10</sup> and anti-inflammatory<sup>11</sup> agents, AChE inhibitors,<sup>12</sup> antimicrobials<sup>13</sup> as well as EP1 receptor antagonists.<sup>14,15</sup> Motivated by the aforementioned findings and pursuing our studies on different five membered heterocycles<sup>16-19</sup> as well as structural studies<sup>20</sup> we have designed new derivatives with pyrazolyl-thiazole moieties (Scheme 2). Similarly in continuation of our recent studies on antiparallel  $\pi$ - $\pi$  interactions in isatin based hydrazides,<sup>21</sup>  $\pi$ -hole tetrel bonding in 2-triazolyl-2-oxoacetate derivatives<sup>22</sup> and recurrent  $\pi$ -stacking motifs in pyrazolyl-thiazole-coumarin hybrids,<sup>23</sup> we report herein synthetic protocols to access aryl-substituted pyrazolyl-thiazole derivatives. The structures reported herein exhibit interesting solid state architectures with an intricate combination of interactions, including

<sup>a</sup> Department of Chemistry, The University of Azad Jammu and Kashmir, Muzaffarabad, 13100 Pakistan

<sup>b</sup> Department of Chemistry, Quaid-i-Azam University, Islamabad 45320, Pakistan

<sup>c</sup> Department of Zoology, The University of Azad Jammu and Kashmir, Muzaffarabad, 13100 Pakistan

<sup>d</sup> Research Laboratory of Bioenergy, Department of Chemistry, Federal Urdu University of Arts, Science and Technology, Gulshan-e-Iqbal Campus, University Road, Karachi- 75300, Pakistan

<sup>e</sup> Department of Physics, University of Sargodha, Sargodha Pakistan

<sup>f</sup> INBIOFAL (CONICET – UNT). Instituto de Química Orgánica. Facultad de Bioquímica, Química y Farmacia. Universidad Nacional de Tucumán. Ayacucho 471. T4000INI. San Miguel de Tucumán. Argentina. diego.gil@fbqf.unt.edu.ar

<sup>g</sup> Department of Química, Universitat de les Illes Balears, Crta. De Valldemossa km 7.5, 07122 Palma de Mallorca (Balears), Spain

Electronic Supplementary Information (ESI) available: Hirshfeld surfaces of compounds **7**, **8** and **10** mapped over Shape Index and Curvedness properties (Fig. S1). See DOI: 10.1039/x0xx00000x

unconventional  $\pi$ -interactions where the non-aromatic pyrazolyl ring is stacked over the aromatic thiazole ring and *vice versa*. Moreover, the role of halogen and chalcogen bonding interactions is also analysed by several computational tools, including molecular electrostatic potential surfaces and a combination of QTAIM and NCIPLOT analyses.

mixture was refluxed till completion (TLC). The mixture was poured into ice cold water and the precipitate was filtered. The solid formed was then recrystallized from  $\text{CHCl}_3$ : EtOH (3:1)<sup>10</sup> to get **10**.

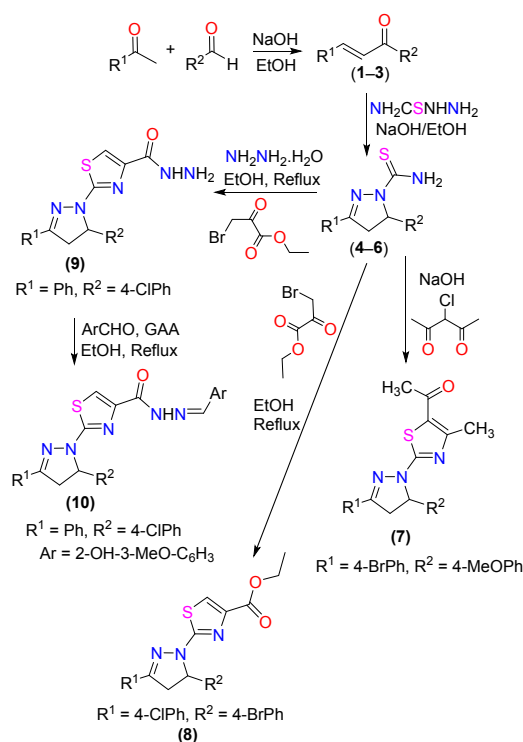
## Experimental and Theoretical Methods

### Instrumentation and Synthesis

All reagents were commercially available and used without further purification. Melting points were determined on a Stuart SMP3 melting point apparatus and are uncorrected. IR spectra were recorded on a Thermo Scientific Nicolet 6700 FTIR spectrophotometer using ATR facility. <sup>1</sup>H and <sup>13</sup>C NMR spectra were recorded on a Bruker Avance 300 MHz instrument in deuterated solvents and the chemical shifts are referenced to TMS. Reactions were monitored using thin layer chromatography (TLC) on silica gel 60F254 coated aluminium sheets (Merck, Germany). X-ray diffractometer analysis was carried out on Bruker Kappa APEX-II CCD diffractometer.

The synthetic route to compounds **4–10** is shown in Scheme 2. By following a procedure already reported in literature<sup>12,24–26</sup> a mixture of substituted acetophenone (5.0 mmol) and 4-substituted benzaldehyde (5.0 mmol) in 20 mL of ethanol (EtOH) was stirred at room temperature followed by the dropwise addition of an aqueous solution of NaOH (10 M). The stirring was continued for 2 h. After reaction completion verified by TLC, the reaction mixture was poured into ice cold water to obtain yellow precipitates. Solid mass was filtered, washed with excess of water and recrystallized from EtOH to get compounds **1–3**. Similarly, compounds **1–3** (1 mmol) and thiosemicarbazide (1 mmol) were dissolved in 20–25 mL of ethanol and stirred vigorously.<sup>12,23</sup> Pellets of NaOH (1.5 mol) were added to the reaction mixture and heated under reflux. After reaction completion (TLC), the suspension was poured into ice cold water. Light yellow precipitates formed were filtered and recrystallized from methanol (MeOH) to give compounds **4–6**. For the synthesis of compound **7**, 2 mmol of **4** (5-dihydro-3, 5-diphenylpyrazole-1-carbothioamide) and 2 mmol of 3-chloropentane-2,4-dione were loaded in 100 mL of RBF. Ethanol was used as solvent. This reaction mixture was stirred for 30 minutes at 50 °C. After completion of reaction, whole mixture was transferred in a beaker having crushed ice. The resulting precipitates were filtered and washed with cold ethanol. After drying, the solid was recrystallized in EtOH:EtOAc 1:1 to get compound **7**.

Compound **4–6** (1.00 mmol) and  $\alpha$ -bromopyruvate (1.0 mmol) were dissolved in ethanol with vigorous stirring at 50–60 °C for 3–4 h. 2,4-Disubstituted-1,3-thiazole **8** precipitate was filtered out and the solid mass obtained was washed with ethanol and recrystallized from  $\text{CHCl}_3$ : EtOH (3:1).<sup>10</sup> Compound **9** (1.0 mmol) and respective benzaldehyde (1 mmol) were added in 20 mL ethanol containing catalytic amount of acetic acid. The reaction



Scheme 2. Synthetic route to compounds 4–10

### 1-(2-(3-(4-Bromophenyl)-5-(4-methoxyphenyl)-4,5-dihydro-1H-pyrazol-1-yl)-4-methylthiazole-5-yl)ethanone (7)

Molecular Formula:  $\text{C}_{22}\text{H}_{20}\text{BrN}_3\text{O}_2\text{S}$ , Mol. Wt. = 470.382, Yellow solid, m.p. = 144–146 °C, Yield = 82%,  $R_f$  = 0.45; IR ( $\bar{\nu}$ , ATR,  $\text{cm}^{-1}$ ): 3122 (Ar-H), 2927 (C-H), 1618 (C=O), <sup>1</sup>H-NMR (300 MHz,  $\text{CDCl}_3$ ) =  $\delta$  ppm 2.45 (3H, s, CH<sub>3</sub>), 2.53 (s, 3H, CH<sub>3</sub>), 3.3 (dd, 1H,  $J_{\text{cis}}$  = 7.2 Hz,  $J_{\text{gem}}$  = 17.4 Hz), 3.8 (s, 3H, -OCH<sub>3</sub>), 4.03 (dd, 1H,  $J_{\text{trans}}$  = 12 Hz,  $J_{\text{gem}}$  = 17.4 Hz), 5.65 (dd, 1H,  $J_{\text{cis}}$  = 7.2 Hz,  $J_{\text{trans}}$  = 12 Hz), 6.92 (m, 2ArH), 7.25 (m, 2ArH), 7.6 (m, 4ArH); <sup>13</sup>C-NMR (75 MHz,  $\text{CDCl}_3$ ):  $\delta$  ppm 18.95, 30.06, 43.46, 56.2, 60.94, 106.8, 114.1, 125.4, 128, 131.4, 131.8, 133, 135.8, 158.7, 151.8, 156.6, 167.6, 189.6;

### Ethyl 2-(5-(4-bromophenyl)-3-(4-chlorophenyl)-4,5-dihydropyrazol-1-yl)thiazole-4-carboxylate (8)

Molecular Formula:  $\text{C}_{21}\text{H}_{17}\text{BrClN}_3\text{O}_2\text{S}$ , Mol. Wt. = 490.80, Yellow solid, m.p. = 149–151 °C, Yield = 75%,  $R_f$  = 0.51; IR ( $\bar{\nu}$ , ATR,  $\text{cm}^{-1}$ ): 3033 (C=C-H), 2985 (C-H), 1698 (C=O), <sup>1</sup>H-NMR (300 MHz,  $\text{CDCl}_3$ ):  $\delta$  = 1.34 (t, 3H, J = 7.2 Hz), 3.32 (dd, 1H,  $J_{\text{cis}}$  = 5.4 Hz,  $J_{\text{gem}}$  = 17.4 Hz), 3.90 (dd, 1H,  $J_{\text{trans}}$  = 12.0 Hz,  $J_{\text{gem}}$  = 17.7 Hz), 4.30 (m, 2H), 5.73 (dd, 1H,  $J_{\text{cis}}$  = 5.7 Hz,  $J_{\text{trans}}$  = 12 Hz), 7.31–7.45 (m, 6 ArH), 7.54 (s, 1H), 7.75–7.79 (m, 2ArH); <sup>13</sup>C-NMR (75 MHz,  $\text{CDCl}_3$ ):  $\delta$  ppm 14.1, 44.4, 61.5, 63.3, 118.9, 126.0, 127.2, 128.9, 129.1, 130.6, 131.2, 133.5, 139.6, 143.8, 152.1, 160.3, 165.8.

### 2-(5-(4-Chlorophenyl)-3-phenyl-4,5-dihydro-1H-pyrazol-1-yl)-N'-(2-hydroxy-3-methoxybenzylidene)thiazole-4-carbohydrazide (10)

Molecular Formula:  $C_{27}H_{22}ClN_5O_3S$ , Mol. Wt. = 532.00, Light yellow solid, m.p. = 220-222 °C, Yield = 65%,  $R_f = 0.52$ ; IR ( $\bar{\nu}$ , ATR,  $cm^{-1}$ ): 3242 (NH), 3014 (C-Aromatic), 2926 (C-Aliphatic), 1702 (C=Oamidic), 1587 (C=N), 1564 (C=C);  $^1H$ -NMR (300 MHz,  $CDCl_3$ ) =  $\delta$  ppm 3.44(dd, 1H,  $J_{cis} = 5.7$  Hz,  $J_{gem} = 18.0$  Hz), 3.81 (s, 3H,  $OCH_3$ ), 3.85 (bs, 1H, OH), 4.12 (dd, 1H,  $J_{trans} = 11.7$  Hz,  $J_{gem} = 18.0$ Hz), 5.76 (dd, 1H,  $J_{cis} = 5.7$ Hz,  $J_{trans} = 11.7$ Hz), 6.85-7.51 (m, 9ArH), 7.72 (s, 1H), 7.80-7.83 (m, 3ArH), 8.67 (1, 1NH), 11.25 (1, 1H);  $^{13}C$ -NMR (75 MHz, DMSO):  $\delta$  ppm 43.4, 56.3, 63.5, 114.4, 116.7, 119.4, 119.5, 121.3, 127.1, 129.1, 129.2, 129.4, 130.8, 131.0, 132.8, 140.7, 145.0, 147.6, 148.4, 154.5, 149.0, 157.3, 164.8.

#### Hirshfeld surface calculations

An analysis of the Hirshfeld surfaces (HS) and the corresponding two-dimensional fingerprint plots (full and decomposed)<sup>27</sup> was carried out employing *CrystalExplorer17.5*<sup>28</sup> program to visualize and quantify different intermolecular interactions. The Hirshfeld surfaces were mapped over  $d_{norm}$  shape index and curvedness properties. The  $d_{norm}$  is a symmetric function of distances to the surface from nuclei inside and outside the HS ( $d_i$  and  $d_e$ , respectively), relative to their respective van der Waals (vdW) radii, which enables identification of the regions of particular importance to intermolecular interactions. The  $d_{norm}$  surfaces were mapped over a fixed color scale of -0.050 au (red) – 0.750 Å au (blue). The shape-index property is based on the local curvature of the surface, and it is especially useful to identify planar  $\pi$ -stacking arrangements.<sup>27a</sup>

The interaction energies were computed using a dispersion-corrected CE-B3LYP/6-31G(d,p) level of theory available in *CrystalExplorer17.5* program.<sup>28</sup> The total energy ( $E_{tot}$ ) is the sum of four main components, including electrostatic ( $E_{ele}$ ), polarization ( $E_{pol}$ ), dispersion ( $E_{dis}$ ), and exchange-repulsion ( $E_{rep}$ ) energies, with scale factors of 1.057, 0.740, 0.871 and 0.618, respectively.<sup>29</sup>

#### Theoretical methods

The DFT calculations presented in the last section of the manuscript were carried out using the Gaussian-16 program<sup>30</sup> at the PBE0<sup>31</sup>-D3<sup>32</sup>/def2-TZVP<sup>33</sup> level of theory and using the crystallographic coordinates. The formation energies of the assemblies were evaluated by calculating the difference between the total energy of the assembly and the sum of the monomers that constitute the assembly, which were kept frozen. The molecular electrostatic potential was computed at the same level of theory and plotted onto the 0.001 a.u. isosurface. The QTAIM<sup>34</sup> distribution of critical points (CPs) and NCI plot<sup>35,36</sup> isosurfaces have been used to characterize non-covalent interactions. They correspond to both favourable and unfavourable interactions, as differentiated by the sign of the second density Hessian eigenvalue and defined by the isosurface colour. The colour scheme is a red-yellow-green-blue scale with red for  $\rho^+_{cut}$  (repulsive) and blue for  $\rho^-_{cut}$  (attractive).

#### X-ray data collection and structure refinement

Suitable single crystals grown from (EtOH:EtOAc) of compounds **7**, **8** and **10** were selected for X-ray analyses and diffraction data were collected on a Bruker Kappa APEX-II CCD detector with

$MoK\alpha$  radiation at 296 K. Semi empirical correction was applied using the SADABS program.<sup>37</sup> All the structures were solved by direct methods using SHELX program.<sup>38</sup> Positions and anisotropic parameters of all non-H atoms were refined on  $F^2$  using the full matrix least-squares technique. The H atoms were added at geometrically calculated positions and refined using the riding model. The details of crystallographic data and crystal refinement parameters for the compounds **7,8,10** are given in Table 1.

## Results and discussion

#### Description of crystal structures of compounds **7**, **8** and **10**.

The molecular structures of compounds **7**, **8** and **10** are shown in Fig. 1. Crystal data and structure refinement are presented in Table 1. Compounds **7** and **8** crystallize in the triclinic crystal system with the centrosymmetric  $P\bar{1}$  space group accommodating two and one molecules per unit cell, respectively. Compound **10** crystallizes in the orthorhombic  $Pca_21$  space group with  $Z = 4$  molecules per unit cell.

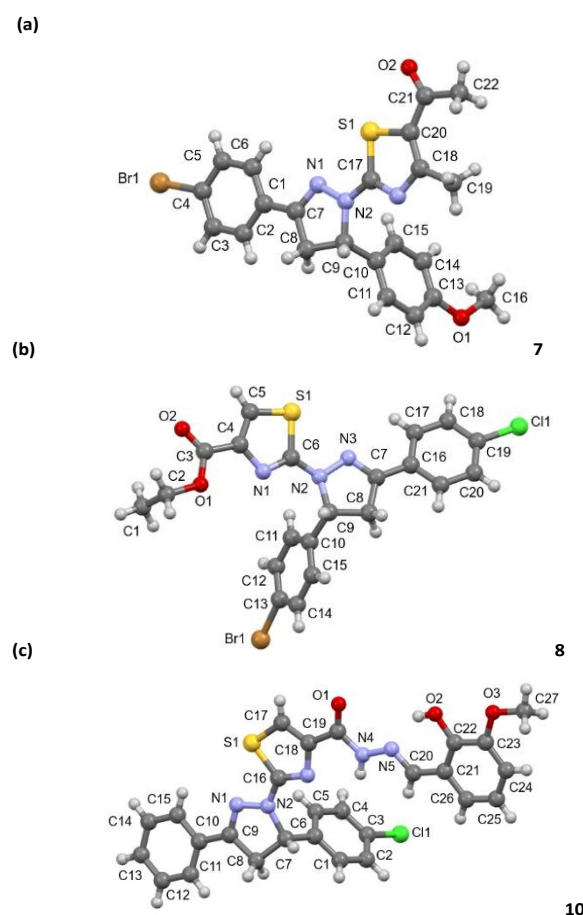


Fig. 1 Molecular structure of compounds **7** (top), **8** (middle) and **10** (bottom). Atoms numbering scheme is also given.

In **7**, the bromophenyl moiety A (C1-C6/Br1), 4,5-dihydro-1H-pyrazole ring B (C7-C9/N1/N2), anisole moiety C (C10-C16/O1) and the 1-(4-methylthiazol-5-yl)ethanone moiety D (C17-C22/N3/O2/S1) are found to be planar with respective root

mean square (r. m. s) deviation of 0.0075, 0.0518, 0.0638 and 0.0179 Å. The dihedral angles A/B, B/C and B/D are 7.52 (8)°, 74.36 (10)° and 6.85 (8)°, respectively. The dihedral angles infer that the moieties A and B are nearly planar to each other and similarly moieties B and D are nearly planar.

In **8** (Fig. 1b, Table 1), methyl thiazole-4-carboxylate moiety A (C2-C6/N1/O1/O2/S1), 4,5-dihydro-1H-pyrazole ring B (C7-C9/N2/N3), bromophenyl ring C (C10-C15/Br1) and chlorophenyl ring D (C16-C21/Cl1) are found to be planar with respective root mean square (r.m.s) deviation of 0.0579, 0.0082, 0.0183 and 0.0108 Å. The central ring B is twisted at respective dihedral angles of 18.8 (2)°, 67.2 (1)° and 6.67 (3)° with respect to moiety A, rings C and D. Chloro-substituted phenyl ring makes dihedral angle of 64.5 (1)° with respect to bromo-substituted ring. This dihedral angles inspection infers that ring B and D are almost parallel. The terminal C-atom (C1) is at the distance of 1.3589 (7) Å from the plane of moiety A.

In **10** (Figure 1c, Table 1), chloro phenyl ring A (C1-C6/Cl1), 4,5-dihydro-1H-pyrazole ring B (C7-C9/N1/N2), phenyl ring C (C10-C15), thiazole ring D (C16-C18/N3/S1), (E)-N'-(2-hydroxy-3-methoxybenzylidene)formohydrazide group E (C19-C27/N4/N5/O1-O3) are found be planar with respective r.m.s deviation of 0.0069, 0.0666, 0.0090, 0.0028 and 0.0156 Å. Thiazole ring D is twisted at dihedral angle of 8.02 (3)° and 1.32 (2)° with respect to ring B and group E, respectively. These dihedral angles infer that thiazole ring D and group E are almost parallel. Chlorophenyl ring A makes dihedral angle of 80.04(1)° and 86.7(9)° with respect to ring C and group E, respectively.

### Crystal packing and interaction energy analysis

The intermolecular interactions which are responsible of the crystal packing of compounds **7**, **8** and **10** are reported in Table 2 along with the respective interaction energies.

The crystal packing of compound **7** is stabilized by both classical and non-classical non covalent interactions including C-H...O, C-H...Br, C-H... $\pi$  and  $\pi$ ... $\pi$  stacking interactions, as can be shown in Fig. 2. The strong dimer D2 ( $E_{\text{tot}} = -22.3$  kcal/mol) is further stabilized by C-H... $\pi$  interactions involving the H6 atom from the bromophenyl ring and the Cg4 centroid of the anisole ring [ $d(\text{H6}\cdots\text{Cg4}) = 3.83$  Å]. In addition, this dimer is stabilized by offset  $\pi$ ... $\pi$  stacking interactions between the centroid of the thiazole ring Cg1 and centroid of the bromophenyl moiety Cg3, with an inter-centroid separation of 3.8853(2) Å (symmetry: 1-x, 2-y, -z) corresponding to ring off-set of 1.573 Å. The contribution of dispersion energy was calculated to be 75.1% towards the stabilization of this structural dimer. The dimer D1 ( $E_{\text{tot}} = -20.6$  kcal/mol) is stabilized by intermolecular C8-H8B...O2 hydrogen bonds involving the O2 atom from the carbonyl group as acceptor and the H8B atom from the 4,5-dihydro-1H-pyrazole ring. The electrostatic and dispersion energies contribute 33.7% and 66.3%, respectively towards the stabilization of this dimer.

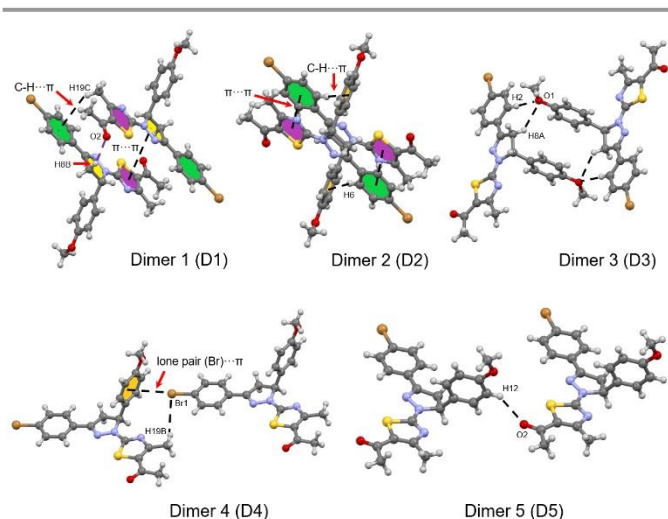
**Table 1.** Crystal data and structure refinement for compounds **7**, **8** and **10**. Article Online DOI: 10.1039/D1CE00256B

Crystal data	<b>7</b>	<b>8</b>	<b>10</b>
CCDC	1981404	1009301	1009302
Chemical formula	C <sub>22</sub> H <sub>20</sub> BrN <sub>3</sub> O <sub>2</sub> S	C <sub>21</sub> H <sub>17</sub> BrClN <sub>3</sub> O <sub>2</sub> S	C <sub>27</sub> H <sub>22</sub> ClN <sub>5</sub> O <sub>3</sub> S
$M_r$	470.38	490.80	532.00
Crystal system, space group	Triclinic $P\bar{1}$	Triclinic $P1$	Orthorhombic $Pca2_1$
Temperature (K)	296	296	296
$a$ (Å)	7.3329(4)	4.7441(4)	23.994(4)
$b$ (Å)	11.3359(7)	9.5883(9)	5.0580(9)
$c$ (Å)	13.3196(7)	12.0770(11)	20.359(3)
$\alpha$ (°)	105.658(3)	73.421	90, 90, 90
$\beta$ (°)	92.689(2)	(5), 89.483	
$\gamma$ (°)	97.255(3)	(5), 86.045 (6)	
$V$ (Å <sup>3</sup> )	1053.76 (10)	525.23 (8)	2470.8 (7)
$Z$	2	1	4
Density	1.482	1.552	1.430
$F(000)$	480	248	1104
Wavelength (Å)	0.71073 Å	0.71073 Å	0.71073 Å
$\mu$ (mm <sup>-1</sup> )	2.073	2.206	0.280
Crystal shape	Needle	Needle	Needle
Crystal Colour	Yellow	White	Light yellow
Crystal size (mm)	0.38 × 0.20 × 0.18	0.40 × 0.18 × 0.16	0.42 × 0.22 × 0.16
No. of measured, independent	15423 4064	8109 4306	20066 5563
And observed [ $I > 2s(I)$ ] reflections	2568	3367	2853
$R_{\text{int}}$	0.037	0.027	0.089
Theta range for data collection	2.788 to 26.000	2.222 to 27.502	1.697 to 27.481
Index ranges	-8 ≤ $h$ ≤ 8 -13 ≤ $k$ ≤ 13 -16 ≤ $l$ ≤ 16	-5 ≤ $h$ ≤ 6 -12 ≤ $k$ ≤ 12 -15 ≤ $l$ ≤ 15	-30 ≤ $h$ ≤ 31 -5 ≤ $k$ ≤ 6 -26 ≤ $l$ ≤ 25
$(\sin \theta/\lambda)_{\text{max}}$ (Å <sup>-1</sup> )	0.617	0.650	
$R[F^2 > 2\sigma(F^2)]$	0.040	0.035	0.047
$wR(F^2)$	0.098	0.077	0.078
$S$	1.02	1.03	0.92
No. of reflections	4064	4306	5563
No. of parameters	265	263	336
No. of restraints	-	3	1
$\Delta\rho_{\text{max}}, \Delta\rho_{\text{min}}$ (e Å <sup>-3</sup> )	0.43, -0.44	0.17, -0.30	0.23, -0.27

Intermolecular C2-H2...O1 and C8-H8A...O1 hydrogen bonding interactions are responsible of the stabilization of dimer D3 ( $E_{\text{tot}} = -12.4$  kcal/mol) with 41.8% of electrostatic energy contribution towards the stabilization.

**Table 2:** Interaction energies (kcal/mol) of the main intermolecular interactions for various molecular pairs observed in the crystal structure of compounds **7**, **8** and **10**.

Dimer	R <sup>a</sup>	Symmetry	Involved interactions <sup>b</sup>	Geometry <sup>c</sup> H...A/ < (D-H...A)	E <sub>ele</sub>	E <sub>pol</sub>	E <sub>dis</sub>	E <sub>rep</sub>	E <sub>tot</sub>
<b>Compound 7</b>									
D1	6.38	-x, -y, -z	C8-H8B...O2 C19-H19C...Cg3 Cg1...Cg2	2.53/149 3.42 4.2636(3)	-9.3	-2.4	-23.0	13.8	-20.6
D2	3.43	-x, -y, -z	C6-H6...Cg4 Cg1...Cg3	3.83 3.8853(2)	-7.2	-2.5	-29.1	15.8	-22.3
D3	9.20	-x, -y, -z	C2-H2...O1 C8-H8A...O1	2.57/174 2.67/127	-5.7	-2.0	-10.7	5.5	-12.4
D4	13.32	x, y, z	Br1...Cg4 C19-H19B...Br1	3.6279(2) 3.35/146	-0.7	-0.2	-5.1	3.3	-2.9
D5	11.34	x, y, z	C12-H12...O2	2.54/143	-1.4	-0.9	-1.7	1.0	-2.7
<b>Compound 8</b>									
D1	4.74	x, y, z	C11-H11...O1 C11-H11...N1 Cg3...Cg3 Cg2...Cg4 Cl1...Cg4	2.68/136 2.83/160 4.7441(4) 4.1285(4) 4.02	-3.6	-2.4	-25.6	10.2	-20.1
D2	10.99	x, y, z	C8-H8B...O2 C5-H5...Cg4	2.51/157 3.50	-3.3	-1.2	-6.8	3.5	-7.3
D3	9.59	x, y, z	C15-H15...O2	2.75/159	-1.8	-1.1	-6.5	3.3	-5.7
D4	12.08	x, y, z	Br1...S1 C17-H17...Br1	3.75 3.49/126	-0.4	0.0	-2.4	1.4	-1.5
<b>Compound 10</b>									
D1	5.06	x, y, z	C5-H5...N3 C27-H27A...O2 C27-H27A...Cg5 C20-H20...Cg3 C8-H8B...Cg4 Cg2...Cg4	2.71/155 2.85/130 3.51 3.22 2.56 3.71	-5.1	-3.4	-36.9	20.3	-24.2
D2	12.66	x+1/2, -y, z	C8-H8A...O3 C27-H27B...Cg3	2.66/149 3.03	-6.0	-2.0	-5.3	1.8	-10.7
D3	12.04	x+1/2, -y, z	C11-H11...O1 C12-H12...O1	2.68/119 2.80/114	-2.4	-1.3	-3.8	1.5	-5.6

**Fig. 2** View of the different dimers observed in the crystal structure of **7**. Intermolecular interactions are shown as dashed lines. Cg1: S1/C17/N3/C18/C20 centroid (violet), Cg2: N1/N2/C7-C9 centroid (yellow), Cg3: C1-C6 centroid (green), Cg4: C10-C15 centroid (orange).

Interestingly, the crystal packing of **7** is further stabilized by (Br1)⋯π interactions involving the Br1 atom and the centroid Cg4 of the anisole ring [ $d(\text{Br}1\cdots\text{Cg}4) = 3.6279(2) \text{ \AA}$ ;  $\langle(\text{C}4\text{-Br}1\cdots\text{Cg}4) = 167.80(1)^\circ$ , symmetry:  $x, y, -1+z$ ] and weak C-H⋯Br hydrogen bonds involving the H19B of the 1-(4-methylthiazol-5-yl)ethanone moiety and the bromine atom of the bromophenyl ring (Dimer 4). The intermolecular interaction energy for dimer D4 being  $-2.9 \text{ kcal/mol}$  and the dispersion energy contributes 84% towards the stabilization of this structural dimer. Further analysis of this dimer is discussed below regarding the physical nature of the Br⋯π interaction (lone pair⋯π vs halogen bond). The energetically weakest dimer D5 ( $E_{\text{tot}} = -2.7 \text{ kcal/mol}$  with 58% contribution of electrostatic energy) is mainly stabilized by C12-H12⋯O2 hydrogen bonds involving the O2 atom of the 1-(4-methylthiazol-5-yl)ethanone moiety as acceptor and the H12 atom from the anisole ring.

The crystal packing of **8** shows four molecular dimers and the intermolecular interaction energy of these dimers are between  $-20.1$  to  $-1.5 \text{ kcal/mol}$ , as shown in Table 2. These dimers are mainly stabilized by C-H⋯O, C-H⋯N and C-H⋯Br hydrogen

bonds (Fig. 3). In addition, C-H $\cdots\pi$ , lone pair (Cl) $\cdots\pi$  and  $\pi\cdots\pi$  stacking interactions are responsible for the stabilization of the crystal lattice. The strongest dimer D1 ( $E_{\text{tot}} = -20.1$  kcal/mol with the contribution of 81% dispersion energy) is stabilized by C11-H11 $\cdots$ O1 [ $d(\text{H11}\cdots\text{O1}) = 2.68$  Å] and C11-H11 $\cdots$ N1 [ $d(\text{H11}\cdots\text{N1}) = 2.83$  Å] hydrogen bonds. This structural dimer is also stabilized by  $\pi\cdots\pi$  stacking interactions involving bromophenyl rings (Cg3) of adjacent molecules with centroid-to-centroid distance of 4.7441(4) Å (symmetry: 1+x, y, z) and between the 4,5-dihydro-1H-pyrazole ring (Cg2) and the chlorophenyl ring (Cg4), with inter-centroid distance Cg2 $\cdots$ Cg4 of 4.1285(4) Å (symmetry: -1+x, y, z). Interestingly, (Cl1) $\cdots\pi$  interactions involving the Cl1 atom and the chlorophenyl ring (Cg4) [ $d(\text{Cl1}\cdots\text{Cg4}) = 4.020$  Å,  $\angle(\text{C19-Cl1}\cdots\text{Cg4}) = 82.2^\circ$ ] stabilize the dimer D1. The dimer D2 ( $E_{\text{tot}} = -7.3$  kcal/mol) is mainly stabilized by intermolecular C-H $\cdots$ O hydrogen bonds involving the O2 atom of the carbonyl group as acceptor and the H8B of the 4,5-dihydro-1H-pyrazole ring. Additionally, to the hydrogen bond, this structural motif is also stabilized by C-H $\cdots\pi$  interactions, involving the H5 atom of the thiazole ring and the chlorophenyl ring (Cg4). The electrostatic and dispersion energies contribute 60 and 40%, respectively, towards the stabilization of this dimer. The carbonyl group is also involved as an acceptor for the intermolecular C15-H15 $\cdots$ O2 hydrogen bond (dimer D3), with a total interaction energy of -5.7 kcal/mol. It is important to emphasize that the contribution of electrostatic (58.2%) and dispersion (41.8%) are similar. Further, dimer D4 is mainly stabilized by weak C17-H17 $\cdots$ Br1 hydrogen bonds and Br1 $\cdots$ S1 chalcogen bond. The classification of the Br $\cdots$ S contact has been analyzed by using NBO analysis (see theoretical section).

The crystal structure of compound **10** is mainly stabilized by intermolecular C-H $\cdots$ N, C-H $\cdots$ O, C-H $\cdots\pi$  and  $\pi\cdots\pi$  interactions, as shown in Fig. 4. The most stabilized molecular dimer D1 ( $E_{\text{tot}} = -24.2$  kcal/mol) is formed by C5-H5 $\cdots$ N3 and C27-H27A $\cdots$ O2 hydrogen bonds and C-H $\cdots\pi$  contacts [C27-H27A $\cdots$ Cg5, C20-H20 $\cdots$ Cg3 and C8-H8B $\cdots$ Cg4].

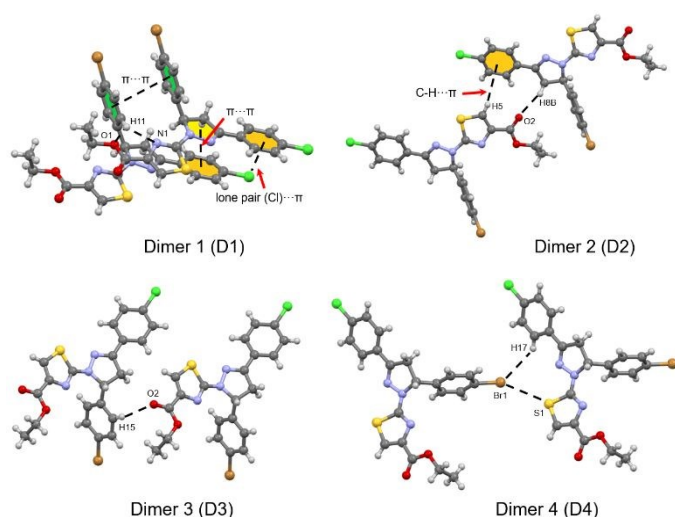


**Figure 3.** Partial view of the different structural dimers observed in the crystal structure of **8**. The intermolecular interactions are shown as dashed lines. Cg2: N1/N2/C7-C9 centroid (yellow), Cg3: C1-C6 centroid (green) and Cg4: C10-C15 centroid (orange).

In addition,  $\pi\cdots\pi$  stacking interactions between 4,5-dihydro-1H-pyrazole (Cg2) and phenyl ring (Cg4) are also responsible for the dimer stabilization. The dispersion energy (81%) is contributing more than 4-fold that of electrostatic energy (19%) towards the stabilization. The dimer D2 is generated by intermolecular C-H $\cdots$ O hydrogen bonding interactions involving the H8A of the 4,5-dihydro-1H-pyrazole ring and the O3 atom of the methoxy group as acceptor [ $d(\text{H8A}\cdots\text{O3}) = 2.66$  Å]. This structural motif is also stabilized by C-H $\cdots\pi$  contacts involving the H27B atom of the methoxy group and the chlorophenyl ring (Cg3), with H27B $\cdots$ Cg3 distance of 3.03 Å. It is important to emphasize that the contribution of electrostatic (60.3%) is higher than dispersion (39.7%) towards the stabilization of dimer D2.

As shown in Fig. 4, the structural dimer D3 ( $E_{\text{tot}} = -5.6$  kcal/mol) is stabilized by two C11-H11 $\cdots$ O1 and C12-H12 $\cdots$ O1 hydrogen bonds. The electrostatic and dispersion energies contribute 49.7 and 50.3%, respectively, towards the stabilization of this dimer.

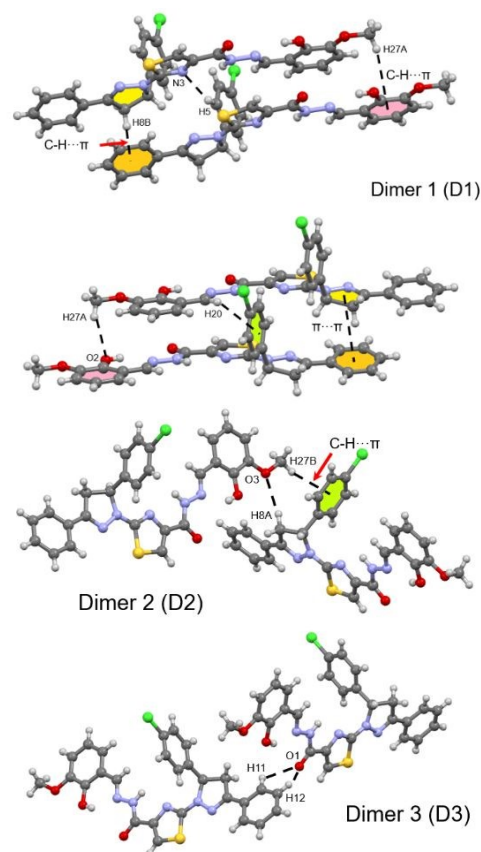


**Fig. 4** Partial view of the different structural dimers observed in the crystal structure of **10**. The intermolecular interactions are shown as dashed lines. Cg2: N1/N2/C7-C9 centroid (yellow), Cg3: C1-C6 centroid (green), Cg4: C10-C15 centroid (orange), and Cg5: C21-C26 centroid (pink).

#### Hirshfeld surface analysis

Hirshfeld surface analysis have been carried out to understand the nature of packing motifs and the contribution of the main intermolecular interactions which are responsible of the supramolecular architectures in crystalline solids **7**, **8** and **10**. Fig. 5 shows Hirshfeld surfaces mapped over  $d_{\text{norm}}$  function,

where arrows with numbers indicate close contacts. Graphical plots of the molecular Hirshfeld surfaces mapped over  $d_{\text{norm}}$  property using a red-white-blue color scheme, where red indicates shorter contacts, white is used for contacts around the van der Waals (vdW) separation, and blue is used for longer contacts. Full and decomposed two-dimensional fingerprint (FP) plots of the main intermolecular contacts are presented in Fig. 6.

In compound **7**, the largest and red regions labeled 1, 2 and 3 in Fig. 5 are attributed to C8-H8B...O2, C2-H2...O1 and C12-H12...O3 hydrogen bonds, respectively. These contacts are represented as a pair of spikes at  $(d_e + d_i) \approx 2.4$  Å in the fingerprint plot (Fig. 6) with a contribution of 12.2% to the total Hirshfeld surface area. Two red spots labeled 4 and 5 (Fig. 5) represent H...C/C...H contacts with large area fraction of 12.3 %.

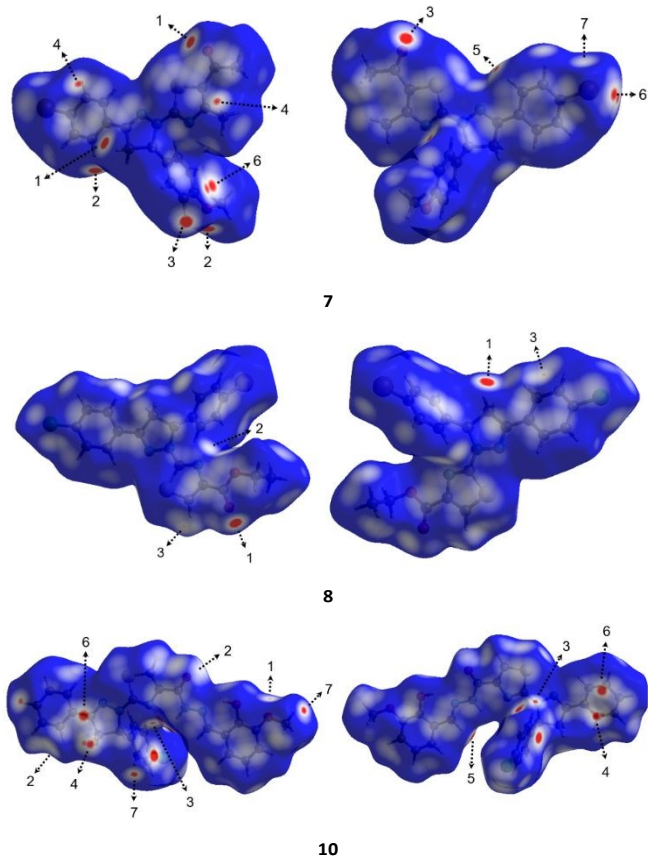


**Fig. 5** Hirshfeld surfaces of compounds **7**, **8** and **10** mapped over  $d_{\text{norm}}$  function in two orientations (the second molecule is rotated 180° around the horizontal axis of the plot). The labels are discussed in the main text.

These contacts are attributed to C19-H19C...Cg3 and C6-H6...Cg4 interactions, which appear in the form of “wings” on the sides of the fingerprint plots (Fig. 6), characteristic of C-H... $\pi$  contacts with the shortest  $(d_e + d_i) \approx 3.2$  Å. The red spots labeled 6 in the  $d_{\text{norm}}$  surface are attributed to lone pair (Br1)... $\pi$  interactions, as was described previously. These contacts are also visible in the FP plots as two broad spikes at  $(d_e + d_i) \approx 3.4$  Å with 3.00 % contribution to the Hirshfeld surface area. The white spot labeled 7 in the  $d_{\text{norm}}$  map show weak H...Br/Br...H contacts attributed to C19-H19B...Br1 hydrogen bonds, which

are viewed as broad spikes at  $(d_e + d_i) \approx 3.0$  Å in the fingerprint plot with a contribution of 9.4% to the Hirshfeld surface area. In compound **8**, the H...O/O...H contacts labeled 1 in Fig. 5 are attributed to C8-H8B...O2 hydrogen bonds. These contacts appear as sharp spikes in FP with short  $(d_e + d_i) \approx 2.3$  Å and a contribution of 8.60 % to the total Hirshfeld surface. The white spot labeled 2 in the  $d_{\text{norm}}$  map is attributed to weak C11-H11...N1 hydrogen bonds, which are viewed as a pair of broad spikes at  $(d_e + d_i) \approx 2.6$  Å in FP with a contribution of 5.4% to the total Hirshfeld surface area.

The occurrence of small red spots (labeled 3) on the Hirshfeld surfaces (Fig. 5) is associated to weak C-H... $\pi$  contacts involving the H5 atom and the Cg4 centroid with high contribution of 17.8 %. The sharp spikes observed in the decomposed FP plot (Fig. 6) with 2.10 % contribution to the total Hirshfeld surface area confirm the relevance of Br...S/S...Br in the supramolecular assembly of compound **8**.

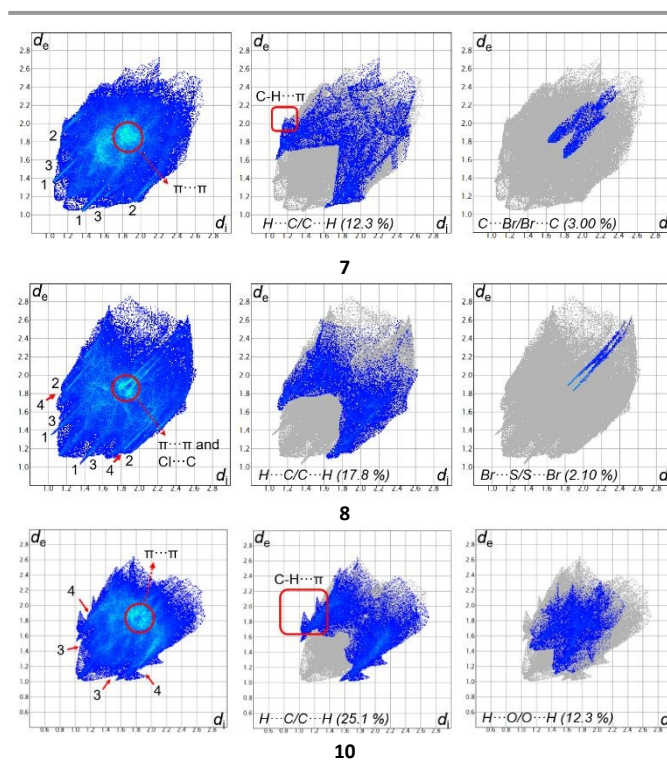


**Fig. 6** Full and decomposed two-dimensional fingerprint plots for compounds **7**, **8** and **10**. Close contacts are labeled as follows: (1) H...O/O...H, (2) H...Br/Br...H, (3) H...N/N...H, (4) H...Cl/Cl...H.

In compound **10**, the small red spots labeled 1 and 2 in the  $d_{\text{norm}}$  map is attributed to C8-H8A...O3 and C11-H11...O1 hydrogen bonds, respectively. These H...O/O...H contacts are visible in the FP plots as two broad spikes at  $(d_e + d_i) \approx 2.5$  Å, comprising a 12.3 % contribution to the Hirshfeld surface area. The red regions labeled 3 in the  $d_{\text{norm}}$  surfaces (Fig. 5) are attributed to C5-H5...N3 hydrogen bonds (Fig. 4), and represented as a pair of broad spikes at  $(d_e + d_i) \approx 2.5$  Å in FP, with a contribution of 4.00 %. Like in structure **7**, the small red spots labeled 3, 4 and 5 indicate weak H...C/C...H contacts corresponding to C-H... $\pi$



interactions (Table 2) which also appear as two types of “wings” in the FP plots with 25.1 % contribution to the Hirshfeld surface area. The spots labeled 6 in Figure 5 are attributed to  $\pi\cdots\pi$  stacking interactions between Cg2 and Cg4 centroids. The Hirshfeld surface of compound **10** also shows two red spots labeled 7 attributed to vdW H1 $\cdots$ H127B interactions.

H $\cdots$ H contacts are also responsible for the crystal packing of the three studied compounds. These interactions are highlighted in the middle of scattered points of FP plots with minimum values of ( $d_e + d_i$ ) in the range 2.05 - 2.30 Å and highest contributions of 43.4 %, 30.4 % and 35.3 % to the total Hirshfeld surface area for compounds **7**, **8** and **10**, respectively.

In addition to the hydrogen bonds described previously, the crystal structure of the three compounds are stabilized by  $\pi\cdots\pi$  stacking interactions, as shown in Table 2. The C $\cdots$ C contacts appear as a distinct pale blue to green area highlighted by a circle at around  $d_e = d_i = 1.8$  Å in the FP plots of the three compounds.

The Hirshfeld surfaces mapped over *Shape Index* and *Curvedness* properties (Fig. S1, ESI) are a very useful tool to identify planar  $\pi\cdots\pi$  stacking interactions.<sup>39</sup> The pattern of touching red and blue triangles on the *Shape Index* surfaces (highlighted as black circles in Fig. S1, ESI) is characteristic of  $\pi\cdots\pi$  stacking arrangements<sup>40</sup> and they are visible in the surfaces of all structures. The mentioned interactions are also visible as relatively large and green flat regions delineated by blue circles on the corresponding *Curvedness* surfaces (Fig. S1, ESI).

#### DFT calculations

The theoretical study is devoted to analyze two types of motifs found in the solid state of these compounds. On one hand the formation of stacked dimers that present numerous interactions due to the non-aromatic nature of the dihydropyrazolyl ring. On the other hand, we focus on the existence of halogen bonding interactions involving the Br and Cl atoms. In case of compound **8**, the formation of a Br $\cdots$ S interaction is further analyzed in terms of a competition between halogen (XB) and chalcogen (ChB) bonding.

We have computed the dimerization energies (PBE0-D3/def2-TZVP), and performed the QTAIM and NCIPLOT index analyses of several dimers of compounds **7**, **8**, **10** retrieved from the X-ray structures. Both computational tools (QTAIM and NCIPLOT) are very convenient to reveal noncovalent interactions. The existence of a bond path and bond critical point (CP) connecting two atoms is an unambiguous indicator of interaction. Moreover, the NCIPLOT analysis gives information regarding the spatial regions between molecules where the interaction is established. Moreover, the color of the isosurface gives valuable information regarding the attractive (blue and green) or repulsive (yellow and red) nature of the interaction.

First of all, we have computed the MEP surfaces of compounds **7**, **8**, **10** in order to investigate the existence of  $\sigma$ -holes in the halogen atoms and the S-atom of the thiazole group. The MEP surfaces are shown in Fig. 7 and it can be observed that the MEP maximum is located at the CH<sub>2</sub> group of the 4,5-dihydropyrazolyl ring in compounds **7** and **8** (+28 kcal/mol) and

it is located at the NH bond of the hydrazido group (+34 kcal/mol) in compound **10**. The MEP minima are located in the O-atoms of the keto (**7**), ester (**8**) or hydrazido (**10**) substituents of the thiazole ring. By using a much reduced energy scale, the existence of  $\sigma$ -holes at the halogen atoms is revealed, as highlighted in Fig. 7. The MEP values at the  $\sigma$ -holes range from 6.5 kcal/mol at Cl of compound **10** to 12 kcal/mol at Br of compound **7**. The MEP value at the  $\sigma$ -hole of the S-atom is significant more intense (+20 kcal/mol) than those at the halogen atoms. Moreover, this  $\sigma$ -hole overlaps with the  $\sigma$ -hole of the adjacent H-atom (see Fig. 7B, left), and consequently, it is more intense than the  $\sigma$ -hole at the Br atom.

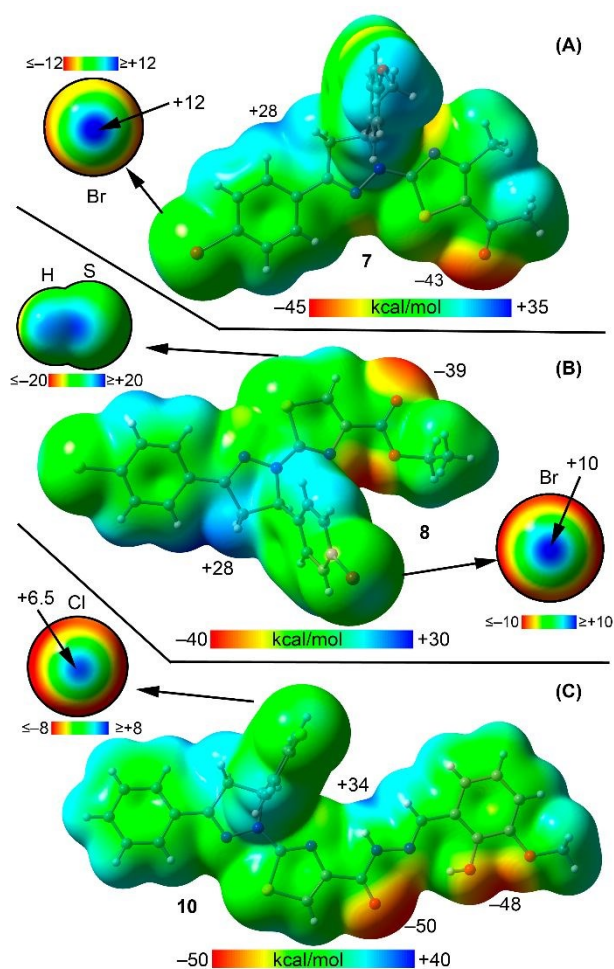
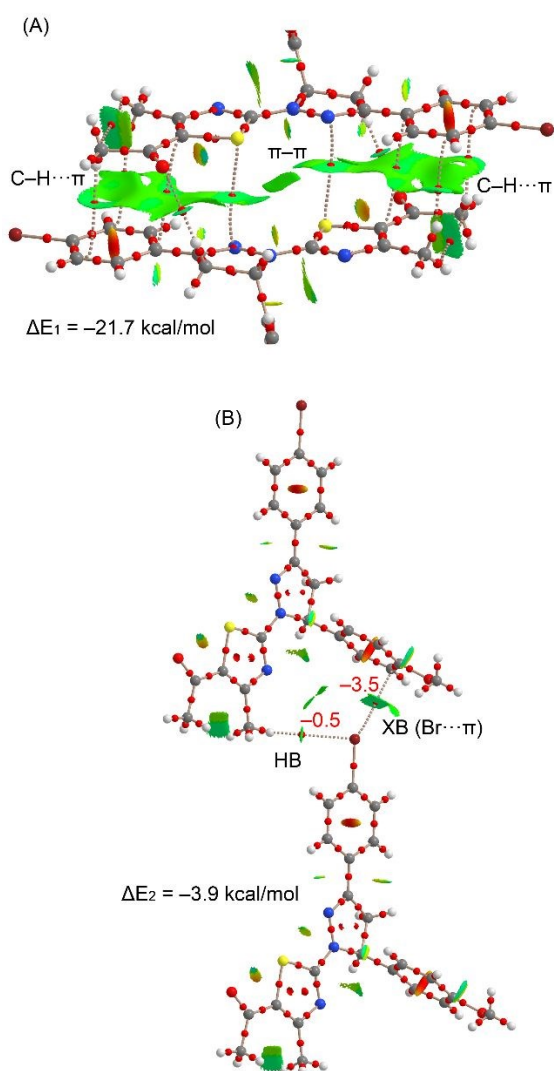


Fig. 7 MEP surfaces (0.001 a.u.) of compounds **7** (A), **8** (B) and **10** (C). The MEP values at selected of the surfaces are indicated in kcal/mol.

Fig. 8 shows the energetic results for the dimers of compound **7** analyzed herein, which consist of the stacked dimer and the halogen bonding complex. The QTAIM analysis of the stacked dimer shows a large number of bond CPs (represented as small red spheres) and bond paths (dashed lines) interconnecting several atoms of both monomers. Moreover, the NCIPLOT shows extended isosurfaces located between the aromatic, nonaromatic and C–H bonds, thus justifying the large dimerization energy (–21.7 kcal/mol) and confirming its importance as strong binding motif in the solid state of **7**. Fig.

8B shows the halogen bonding contact where the electron donor moiety is the electron rich  $\pi$ -system of the methoxybenzene ring. The XB is characterized by a bond CP and bond path connecting the Br-atom to one carbon atom of the ring. Moreover, the presence of a green NCIPLOT isosurface between the Br-atom and the aromatic ring further confirms the existence of the XB interaction ( $\text{Br}\cdots\pi$ ). The combined QTAIM/NCIPLOT analysis also reveals the existence of a weak HB between the methyl group and the negative belt of the Br-atom. The dimerization energy is very modest ( $\Delta E_2 = -3.9$  kcal/mol) in line with the small MEP value at the  $\sigma$ -hole (see Fig. 8A). In order to investigate the relative importance of both interactions, we have evaluated the individual interaction energies using the QTAIM potential energy density ( $V_r$ ) predictor measured at the bond CP, as described in the literature (see red numbers in Fig. 8B).<sup>41,42</sup> It can be observed that the XB is stronger than the HB.



**Fig. 8** Combined QTAIM/NCIPLOT analyses of the stacked dimer (A) and the  $\sigma$ -hole complex (B) for compound **7**. Only bond critical points are represented (as red spheres), for the sake of clarity. For the NCIPLOT isosurface (0.5 a.u.), the  $-0.35 < \text{sign}(\lambda_2)\rho < 0.35$  color scale was used. Gradient cut-off = 0.04 a.u.

The sum of the individual energies computed using the  $V_r$  predictor ( $-4.0$  kcal/mol) are very similar to the dimerization energy ( $-3.9$  kcal/mol) computed using the supramolecular approach (energy difference between the complex and the sum of the energies of the monomers), thus giving reliability to the QTAIM energy predictor.

Fig. 9 gathers the results for compound **8** that are similar to those of compound **7** regarding the interaction energies of the stacked ( $-21.4$  kcal/mol) the  $\sigma$ -hole ( $-2.3$  kcal/mol) dimers. The combined QTAIM/NCIPLOT analysis shows that several bond CPs and bond paths interconnect both monomers and extended NCIPLOT isosurfaces located between the aromatic, nonaromatic and C-H bonds. Fig. 9B shows the halogen/chalcogen bonding contact where it is not evident which atom is acting as electron donor and which one is the  $\sigma$ -hole donor. This contact is characterized by a bond CP, bond path connecting the Br-atom to the S-atom of the thiazole ring. Moreover, the presence of a green NCIPLOT isosurface between both atoms further confirms the existence of the interaction (XB or ChB). The combined QTAIM/NCIPLOT analysis also reveals the existence of a weak HB between one aromatic H-atom and the negative belt of the Br-atom. The dimerization energy is very modest ( $\Delta E_4 = -2.3$  kcal/mol) and the evaluation of the individual interaction energies using the  $V_r$  predictor demonstrates that the HB is the weakest interaction.

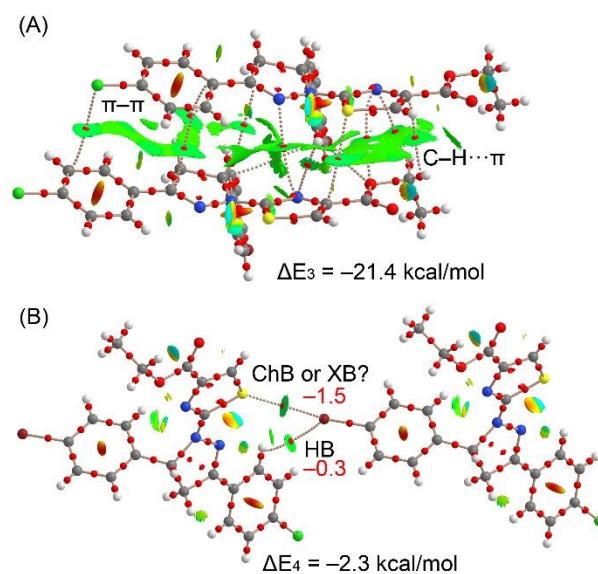


**Fig. 9** Combined QTAIM/NCIPLOT analyses of the stacked dimer (A) and the  $\sigma$ -hole complex (B) for compound **8**. Only bond critical points are represented (as red spheres), for the sake of clarity. For the NCIPLOT isosurface (0.5 a.u.), the  $-0.35 < \text{sign}(\lambda_2)\rho < 0.35$  color scale was used. Gradient cut-off = 0.04 a.u.

In order to classify the  $\text{Br}\cdots\text{S}$  contact we have performed the natural bond orbital (NBO)<sup>43</sup> analysis, focusing on the second order perturbation analysis, since it is very convenient to explore donor-acceptor interactions. Remarkably, we have not found any contribution involving the  $\sigma^*(\text{Br}-\text{C})$  orbital as acceptor, thus ruling out the halogen bond. In contrast, we have found an orbital donor-acceptor interaction from the LP at the Br atom to the antibonding S-C orbital of the thiazole ring, that

is  $Lp(Br) \rightarrow \sigma^*(S-C)$  with a concomitant stabilization energy of 0.30 kcal/mol. Therefore, around of 20% of the ChB energy is due to orbital effects.

Finally, a similar study has been performed for compound **10** and the results are gathered in Fig. 10. Again the stacked dimer presents a very large binding energy due to the large overlap of both molecules, as revealed by the NCIPLOT. In fact, the interaction energy is stronger than those observed for the dimers of **7** and **8** commented above, due to presence of the additional methoxyphenol ring. However, the halogen bonding complex is weaker than those of **7** and **8**, likely due to the fact the Cl instead of Br acts as  $\sigma$ -hole donor, in agreement with the MEP surface analysis. The XB is characterized by a bond CP and bond path interconnecting the Cl and O-atoms. Moreover, the QTAIM also shows the existence of an ancillary H-bond where the negative belt of Cl acts as electron donor. This HB is weaker than the XB, as evidenced by the  $V_r$  energy predictor.

weak  $\sigma$ -hole halogen bonds has been evidenced in these compounds, and in the case of compound **8**, where an ambiguous  $Br \cdots S$  is established, the NBO analysis confirms that the interactions is a chalcogen bond where the Br atom acts as electron rich atom [ $Lp(Br) \rightarrow \sigma^*(S-C)$ ].

## Author Contributions

M.M, S.A., S.H., A.M.K., M.A. and M.M.T.: experimental work, investigation and formal analysis. D.M.G.: Hirshfeld surface analysis; Visualization; Writing – review & editing; Funding acquisition. M.N.A. and A.F.: Formal analysis; Funding acquisition; Methodology; Project administration; Resources; Supervision; Validation; Visualization; Writing – original draft; Writing – review & editing

## Conflicts of interest

There are no conflicts to declare

## Acknowledgements

MNA and MM are thankful to The University of Azad Jammu and Kashmir and Quaid-i-Azam University Islamabad Pakistan for financial support. DMG thanks to ANPCyT (PICT 2016-0226) and SCAIT-UNT (Project 683) and AF thanks to MICIU/AEI, grant number CTQ2017-85821-R, FEDER funds.

## Notes and references

- 1 N. Bakthavatchala Reddy, G. V. Zyryanov, G. Mallikarjuna Reddy, A. Balakrishna, A. Padmaja, V. Padmavathi, C. Suresh Reddy, J. R. Garcia and G. Sravya, *J. Heterocyclic Chem.*, 2019, **56**, 589-596.
- 2 P. Sharma, K. R. Senwar, M. K. Jeengar, T. S. Reddy, V. Naidu, A. Kamal and N. Shankaraiah, *Eur. J. Med. Chem.*, 2015, **104**, 11-24.
- 3 V. Kumar, K. Kaur, G. K. Gupta and A. K. Sharma, *Eur. J. Med. Chem.*, 2013, **69**, 735-753.
- 4 A. Ansari, A. Ali and M. Asif, *New J. Chem.*, 2017, **41**, 16-41.
- 5 A. M. Isloor, B. Kalluraya and P. Shetty, *Eur. J. Med. Chem.*, 2009, **44**, 3784-3787.
- 6 A. Isloor, B. Kalluraya, M. Rao and A. Rahiman, *J. Saudi Chem. Soc*, 2000, **4**, 265-270.
- 7 D. Sunil and P. Shetty, *Der Pharma Chem.*, 2009, **1**, 19-26.
- 8 M. Cuenca-Estrella, A. Gomez-Lopez, E. Mellado, G. Garcia-Effron and J. L. Rodriguez-Tudela, *Antimicrobial. Agents Chemotherapy*, 2004, **48**, 3107-3111.
- 9 R. M. Mohareb, M. Y. Zaki and N. S. Abbas, *Steroids*, 2015, **98**, 80-91.
- 10 M. Madni, S. Hameed, M. N. Ahmed, M. N. Tahir, N. A. Al-Masoudi and C. Pannecouque, *Med. Chem. Res.*, 2017, **26**, 2653-2665.
- 11 P. Kumar, N. Chandak, P. Kaushik, C. Sharma, D. Kaushik, K. R. Aneja and P. K. Sharma, *Med. Chem. Res.*, 2012, **21**, 3396-3405.
- 12 M. Madni, M. N. Ahmed, S. Hameed, S. W. A. Shah, U. Rashid, K. Ayub, M. N. Tahir and T. Mahmood, *J. Mol. Struct.*, 2018, **1168**, 175-186.

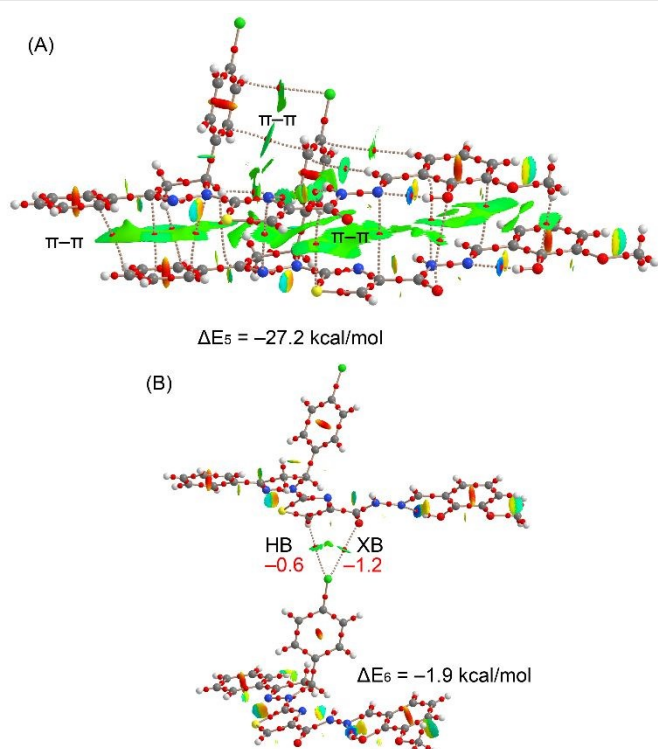


**Fig. 10** Combined QTAIM/NCIplot analyses of the stacked dimer (A) and the  $\sigma$ -hole complex (B) for compound **10**. Only bond critical points are represented (as red spheres), for the sake of clarity. For the NCIplot isosurface (0.5 a.u.), the  $-0.35 < \text{sign}(\lambda_2)\rho < 0.35$  color scale was used. Gradient cut-off = 0.04 a.u.

## Concluding remarks

Three new derivatives of 4,5-dihydropyrazolylthiazole have been synthesized and characterized. The supramolecular assemblies observed in their solid state structure have been analyzed using, Hirshfeld surface analysis, DFT calculations and a combination of QTAIM and NCIPLOT computational tools. All methods suggest that the  $\pi \cdots \pi$  stacking interactions are the most dominant interactions and they have a prominent role directing the X-ray packing in all complexes. The existence of

- 13 H. Patel, V. Ugale, A. Ingale and S. Bari, *Lett. Drug Des. Discovery*, 2012, **9**, 840-847.
- 14 M. Atobe, K. Naganuma, M. Kawanishi, A. Morimoto, K.-i. Kasahara, S. Ohashi, H. Suzuki, T. Hayashi and S. Miyoshi, *Bioorg. Medicinal Chem. Lett.*, 2013, **23**, 6569-6576.
- 15 M. Atobe, K. Naganuma, M. Kawanishi, A. Morimoto, K.-i. Kasahara, S. Ohashi, H. Suzuki, T. Hayashi and S. Miyoshi, *Bioorg. Medicinal Chem. Lett.*, 2013, **23**, 6064-6067.
- 16 M. N. Ahmed, K. A. Yasin, K. Ayub, T. Mahmood, M. N. Tahir, B. A. Khan, M. Hafeez and M. Ahmed, *Journal of Molecular Structure*, 2016, **1106**, 430-439.
- 17 M. N. Ahmed, K. A. Yasin, S. Hameed, K. Ayub, I.-u. Haq, M. N. Tahir and T. Mahmood, *J. Mol. Struct.*, 2017, **1129**, 50-59.
- 18 M. N. Ahmed, B. Sadiq, N. A. Al-Masoudi, K. A. Yasin, S. Hameed, T. Mahmood, K. Ayub and M. N. Tahir, *J. Mol. Struct.*, 2018, **1155**, 403-413.
- 19 B. Wang, M. N. Ahmed, J. Zhang, W. Chen, X. Wang and Y. Hu, *Tetrahedron Lett.*, 2013, **54**, 6097-6100.
- 20 M. N. Ahmed, K. Ahmad, K. A. Yasin, T. Farooq, B. A. Khan and S. K. Roy, *New J. Chem.*, 2019, **43**, 11316-11333.
- 21 M. N. Ahmed, M. Arif, F. Jabeen, H. A. Khan, K. A. Yasin, M. N. Tahir, A. Franconetti and A. Frontera, *New J. Chem.*, 2019, **43**, 8122-8131.
- 22 M. N. Ahmed, K. A. Yasin, S. Aziz, S. U. Khan, M. N. Tahir, D. M. Gil and A. Frontera, *CrystEngComm*, 2020, **22**, 3567-3578.
- 23 M. Madni, M. N. Ahmed, M. Hafeez, M. Ashfaq, M. N. Tahir, D. M. Gil, B. Galmés, S. Hameed and A. Frontera, *New J. Chem.*, 2020, **44**, 14592-14603.
- 24 M. Madni, S. Hameed, M. N. Ahmed, K. A. Yasin and M. N. Tahir, *Chinese J. Struct. Chem.*, 2015, **7**, 1013-1018.
- 25 Y.-M. Lin, Y. Zhou, M. T. Flavin, L.-M. Zhou, W. Nie and F.-C. Chen, *Bioorg. Med. Chem.*, 2002, **10**, 2795-2802.
- 26 B. F. Abdel-Wahab, H. A. Abdel-Aziz and E. M. Ahmed, *Eur. J. Med. Chem.*, 2009, **44**, 2632-2635.
- 27 (a) J. J. McKinnon, M. A. Spackman and A. S. Mitchell, *Acta Cryst.*, 2004, **60B**, 627-668; (b) J. J. McKinnon, D. Jayatilaka and M. A. Spackman, *Chem. Comm.*, 2007, 3814-3816; (c) M. A. Spackman and D. Jayatilaka, *CrystEngComm*, 2009, **11**, 19-32; (d) M. A. Spackman, *Chem. Rev.*, 1992, **92**, 1769-1797; (e) M. A. Spackman, *Phys. Scr.*, 2013, **87**, 048103.
- 28 M. J. Turner, J. J. McKinnon, S. K. Wolf, D. J. Grimwood, P. R. Spackman, D. Jayatilaka and M. A. Spackman, *CrystalExplorer17* (2017). University of Western, Australia.
- 29 C. F. Mackenzie, P. R. Spackman, D. Jayatilaka, M. A. Spackman, *IUCr* 2017, **4**, 575-587.
- 30 Gaussian 16, Revision C.01, M. J. Frisch, G. W. Trucks, H. B. Schlegel, G. E. Scuseria, M. A. Robb, J. R. Cheeseman, G. Scalmani, V. Barone, G. A. Petersson, H. Nakatsuji, X. Li, M. Caricato, A. V. Marenich, J. Bloino, B. G. Janesko, R. Gomperts, B. Mennucci, H. P. Hratchian, J. V. Ortiz, A. F. Izmaylov, J. L. Sonnenberg, D. Williams-Young, F. Ding, F. Lipparini, F. Egidi, J. Goings, B. Peng, A. Petrone, T. Henderson, D. Ranasinghe, V. G. Zakrzewski, J. Gao, N. Rega, G. Zheng, W. Liang, M. Hada, M. Ehara, K. Toyota, R. Fukuda, J. Hasegawa, M. Ishida, T. Nakajima, Y. Honda, O. Kitao, H. Nakai, T. Vreven, K. Throssell, J. A. Montgomery, Jr., J. E. Peralta, F. Ogliaro, M. J. Bearpark, J. J. Heyd, E. N. Brothers, K. N. Kudin, V. N. Staroverov, T. A. Keith, R. Kobayashi, J. Normand, K. Raghavachari, A. P. Rendell, J. C. Burant, S. S. Iyengar, J. Tomasi, M. Cossi, J. M. Millam, M. Klene, C. Adamo, R. Cammi, J. W. Ochterski, R. L. Martin, K. Morokuma, O. Farkas, J. B. Foresman, and D. J. Fox, Gaussian, Inc., Wallingford CT, 2016.
- 31 C. Adamo and V. Barone, *J. Chem. Phys.*, 1999, **110**, 6158-6169.
- 32 S. Grimme, J. Antony, S. Ehrlich and H. Krieg, *J. Chem. Phys.*, 2010, **132**, 154104
- 33 (a) F. Weigend and R. Ahlrichs, *Phys. Chem. Chem. Phys.*, 2005, **7**, 3297-3305; (b) F. Weigend, *Phys. Chem. Chem. Phys.*, 2006, **8**, 1057-1065.
- 34 R. F. W. Bader, *Chem Rev.*, 1991, **91**, 893-928.
- 35 J. Contreras-Garcia, E. R. Johnson, S. Keinan, R. Chaudret, J. P. Piquemal, D. N. Beratan and W. Yang, *J. Chem. Theory Comput.*, 2011, **7**, 625-532.
- 36 E. R. Johnson, S. Keinan, P. Mori-Sanchez, J. Contreras-Garcia, A. J. Cohen and W. Yang, *J. Am. Chem. Soc.*, 2010, **132**, 6498.
- 37 G. M. Sheldrick, SADABS, Program for empirical X-ray absorption correction; Bruker-Nonius: Madison, WI, 1990.
- 38 G. M. Sheldrick, *Acta Cryst.*, 2015, **C71**, 3-8.
- 39 A. Di Santo, G. A. Echeverría, O. E. Piro, H. Pérez, A. Ben Altabef and D. M. Gil, *J. Mol. Struct.*, 2017, **1134**, 492-503.
- 40 M. A. Spackman and D. Jayatilaka, *CrystEngComm* 2009, **11**, 19-32.
- 41 E. Espinosa, E. Molins and C. Lecomte, *Chem. Phys. Lett.*, 1998, **285**, 170-173.
- 42 A. Bauzá and A. Frontera, *ChemPhysChem*, 2020, **21**, 26-31.
- 43 F. Weinhold, *J. Comp. Chem.* 2012, **33**, 2363-2379.